Supporting Information

Constructing a continuous gradient structure significantly enhances the high-temperature energy storage performance of cellulose acetate multilayer composite films

Fan Zhang, Rui Luo, Nan Zhang, Jing-hui Yang, Yong Wang*

School of Chemistry, Key Laboratory of Advanced Technologies of Materials (Ministry of Education), Southwest Jiaotong University, Chengdu, 610031, China.[1]

- **Note S1.**

Two-parameter Weibull statistic

The characteristic breakdown strength of different dielectric films was analyzed by a two-parameter Weibull statistic:[1]

$$P(E) = 1 - exp(-\frac{E}{E_b})^{\beta} \quad (1)$$

where $P(E)$ is accumulative fault percentage, and β reflects the distribution extent of evaluated breakdown electric field. The larger β value corresponds to more tightly clustered E, implying the superior consistency of the film.

- **Note S2.**

Arrhenius equation

To better understand the electrical breakdown behavior of composite films, the activation energy (E_a) in pure CA and 0.5-1-2 composite film was also calculated according to the Arrhenius equation. The results exhibit a powerful temperature-dependent, and this relationship is calculated by the subsequent formula:[2]

$$\sigma(T) = \sigma_0 exp(-\frac{E_a}{k_B T}) \quad (2)$$

where σ_0 is the precognitive factor, demonstrating under the high-temperature limit of conductivity,

*Corresponding author:
E-mail: yongwang1976@swjtu.edu.cn (Y. Wang)

while T and k_B represent the absolute temperature and the Boltzmann constant, respectively.

- **Note S3.**

Electric conduction modeling

The conduction mechanisms of dielectric polymer films typically fall into two categories: electrode-limited and bulk-limited processes. Electrode-limited conduction includes Schottky emission and Fowler-Nordheim tunneling. In contrast, bulk-limited conduction comprises ohmic conduction, Poole-Frenkel emission, and space-charge-limited transport. Hopping conduction is another essential bulk-limited process.[3,4] In recent years, Schottky emission and hopping conduction have been widely used to explore the conduction mechanism of polymer dielectrics at high temperatures and high fields.

Schottky emission involves electrons in the metal electrodes that gain energy through thermal activation. This energy enables them to surmount the barrier at the metal–dielectric interface and enter the dielectric material. Subsequently, these electrons contribute to the formation of a conduction current.[5]

$$J(E,T) = AT^2 exp\left(\frac{-q(\Phi_s - \sqrt{qE/4\pi\varepsilon_r\varepsilon_0})}{k_B T}\right) \quad (3)$$

where A is the Richardson constant, T represents the absolute temperature, q denotes the electronic charge, $q\Phi_s$ is the Schottky barrier height, ε_r is the optical dielectric constant and k_B is the Boltzmann constant.

Hopping conduction is a tunneling phenomenon where electrons trapped within a dielectric film “hop” between trap sites. Poole-Frenkel emission is analogous to the thermionic effect, where carriers can surmount the trap barrier. In contrast, hopping conduction aligns with the tunneling mechanism. Even when the carrier energy is lower than the maximum energy barrier between trapping sites, carriers can still transition through the dielectric material via the tunneling effect. The J is given by:[6]

$$J(E,T) = 2ne\lambda V \times exp\left(\frac{-E_a}{k_B T}\right) \times sinh\left(\frac{\lambda eE}{2k_B T}\right) \quad (4)$$

where n and V are the carrier concentration and attempt-toescape frequency, e is the charge carrier.

Equation (6) is simplified as:

$$J(E) = A \times sinh(BE) \tag{5}$$

here, A and B are two lumped parameters.

- **Supplemented Figures**

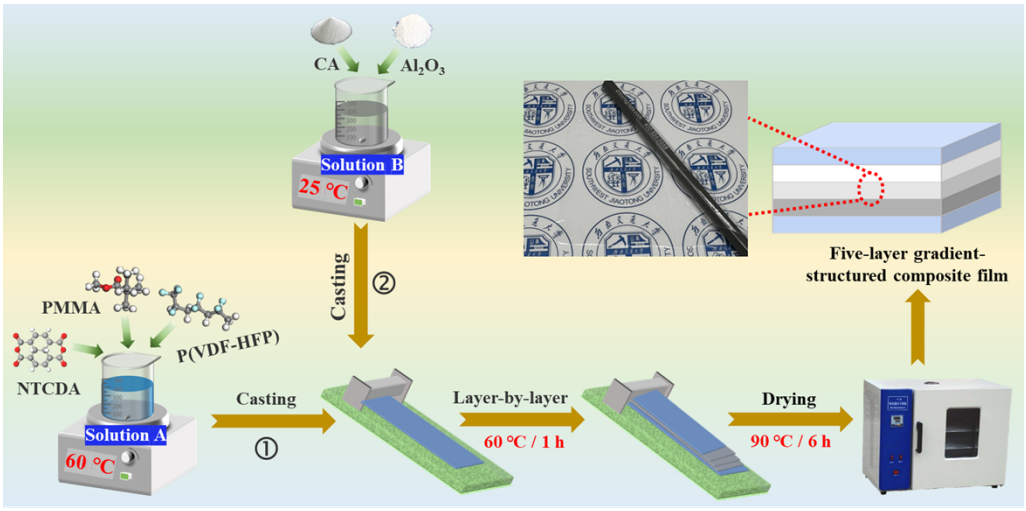

Fig. S1 Schematic diagram showing the fabrication procedures of the five-layer CA-based composite films.

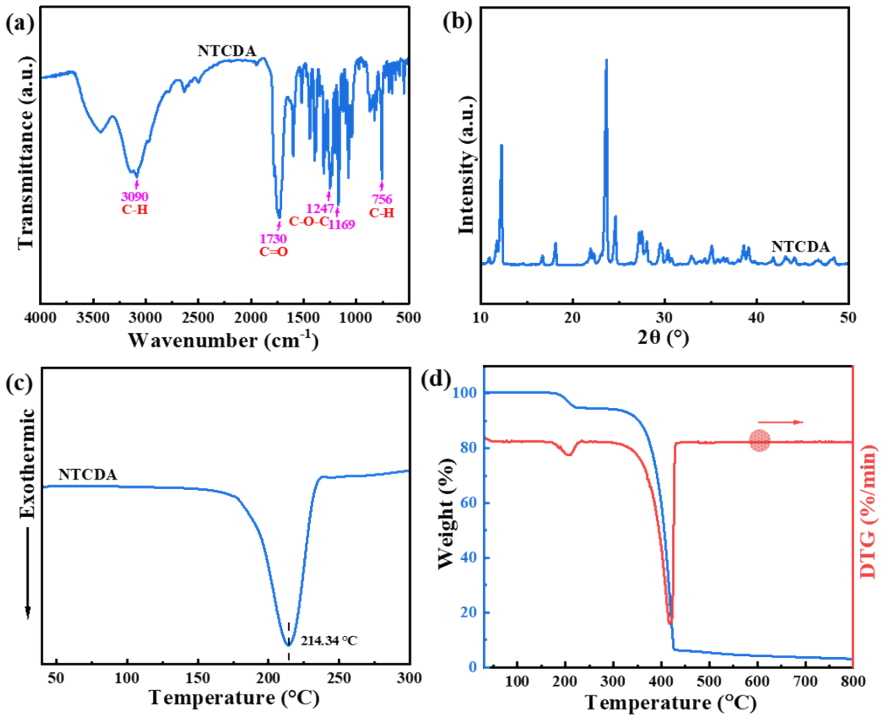

Fig. S2 (a) FTIR spectra, (b) XRD patterns, (c) DSC curve, (d) TGA and DTG curves of NTCDA.

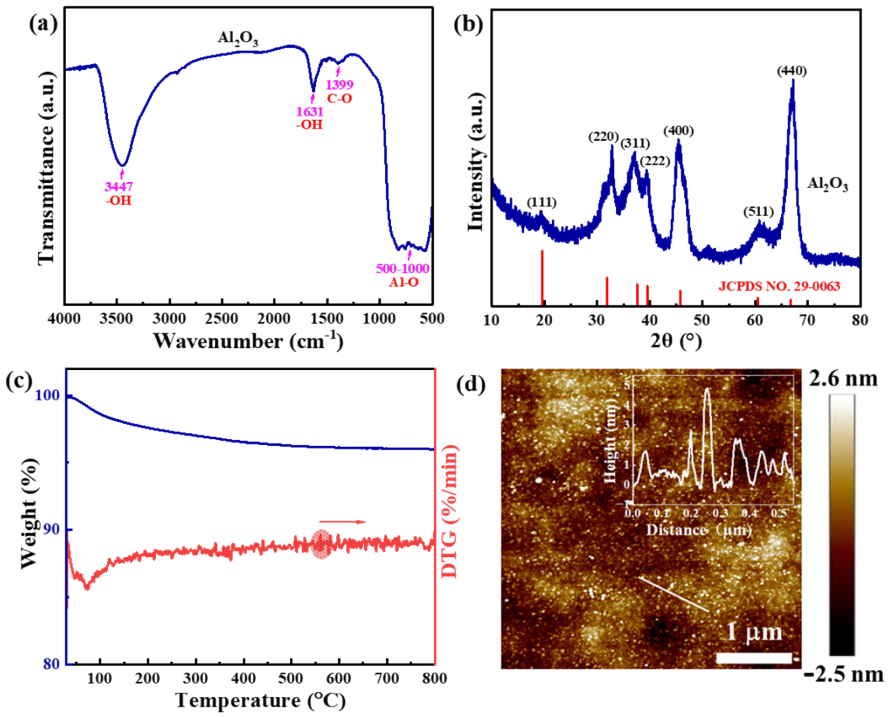

Fig. S3 (a) FTIR spectra, (b) XRD patterns, (c) TGA and DTG curves and (d) AFM images and height profiles of Al_2O_3.

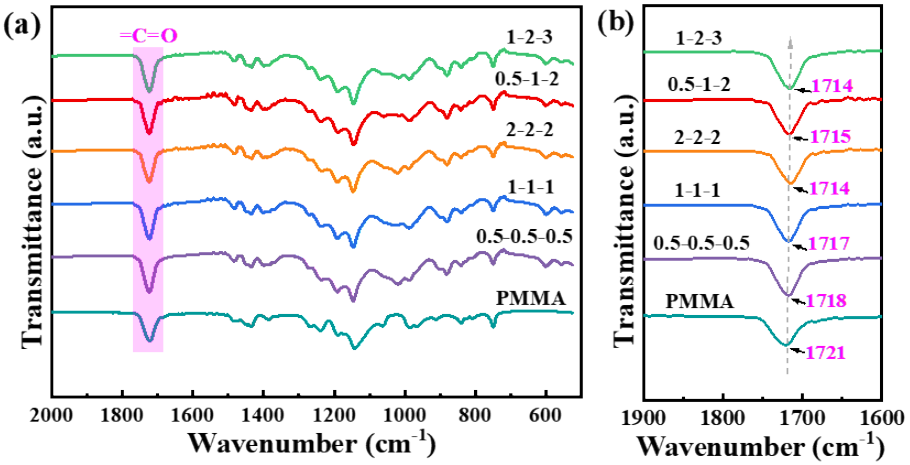

Fig. S4 FTIR spectra of PMMA and various composite films.

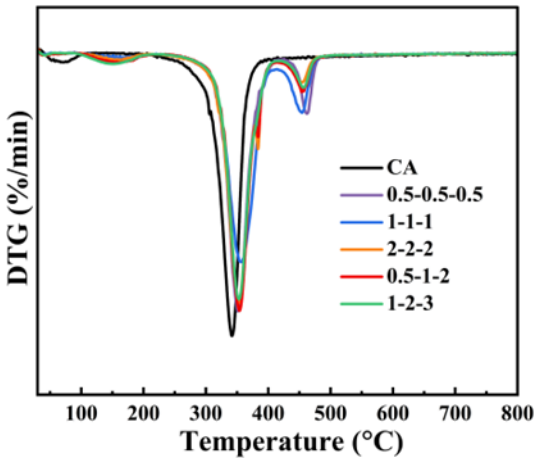

Fig. S5 DTG curves of various composite films.

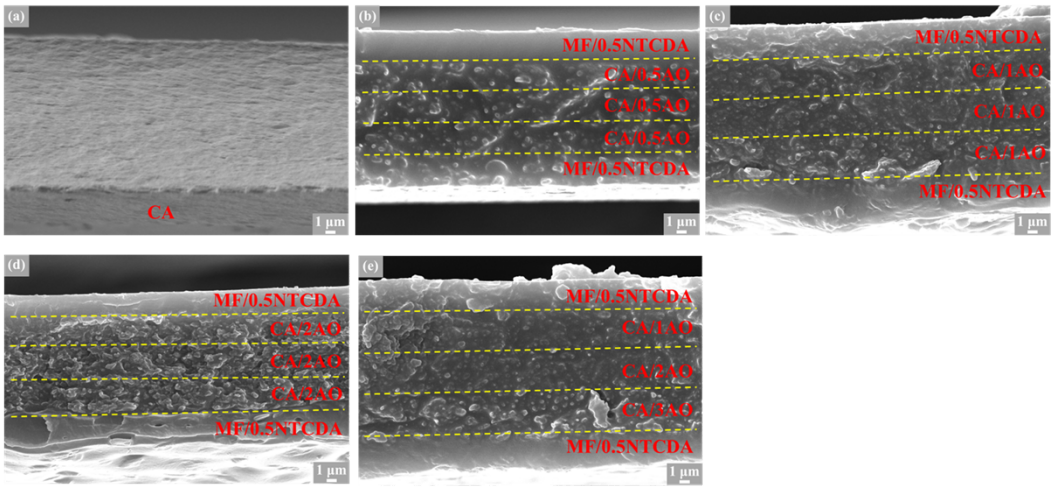

Fig. S6 SEM images showing the cross-sectional morphologies of pure CA film and other composite films as indicated.

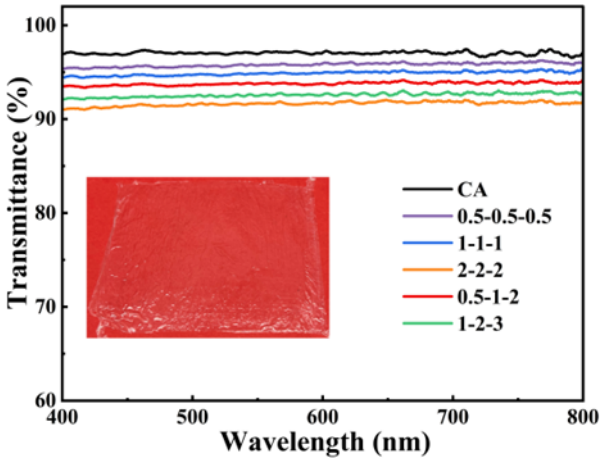

Fig. S7 Light transmittance spectra of the different composite films (the insert image is the photograph of the 0.5-1-2 composite film with high transparency).

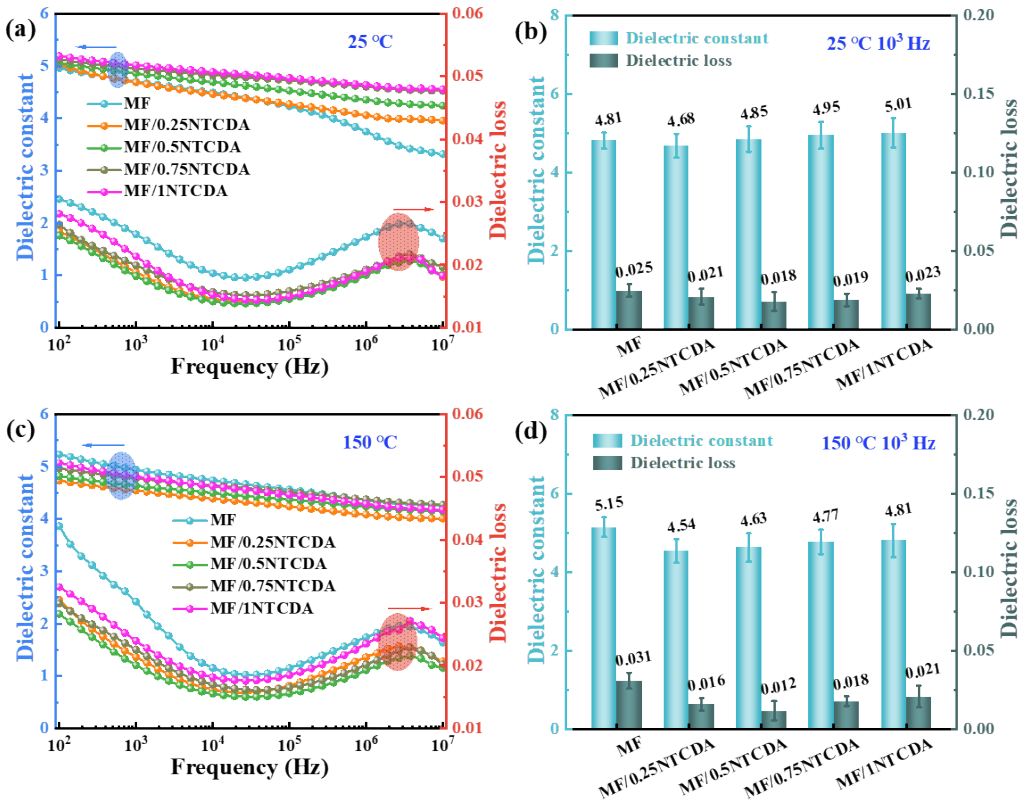

Fig. S8 (a, c) Dielectric properties and (b, d) comparison of dielectric properties among different samples as indicated.

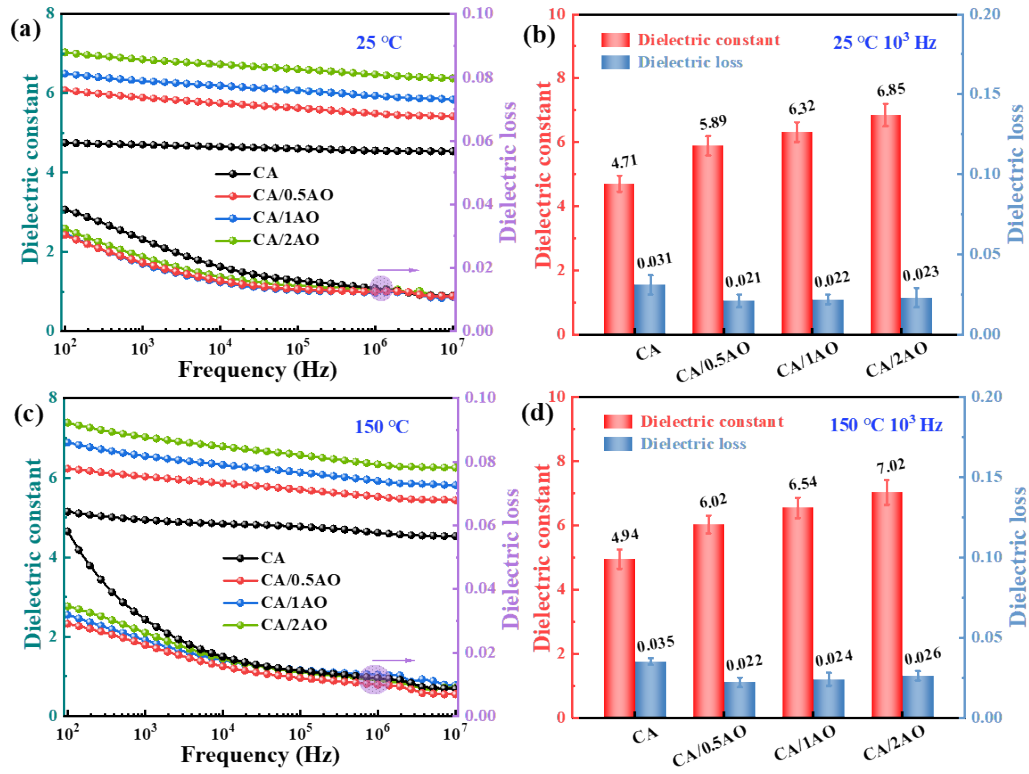

Fig. S9 (a, c) Dielectric properties and (b, d) comparison of dielectric properties among different samples as indicated.

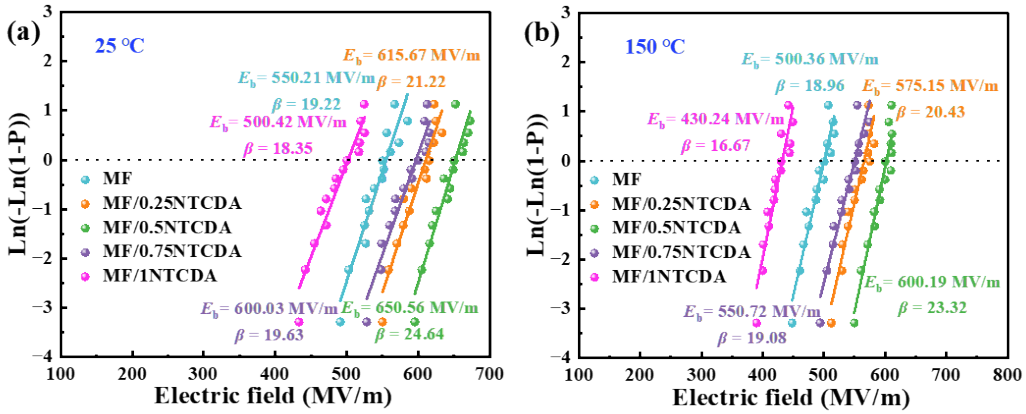

Fig. S10 Weibull distribution analysis of the E_b for different films at (a) 25 ℃ and (b) 150 ℃ as indicated.

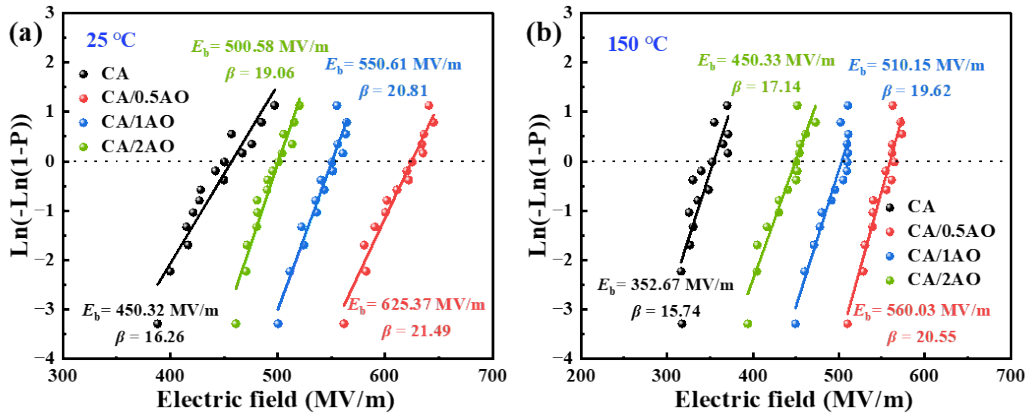

Fig. S11 Weibull distribution analysis of the E_b for different films at (a) 25 ℃ and (b) 150 ℃ as indicated.

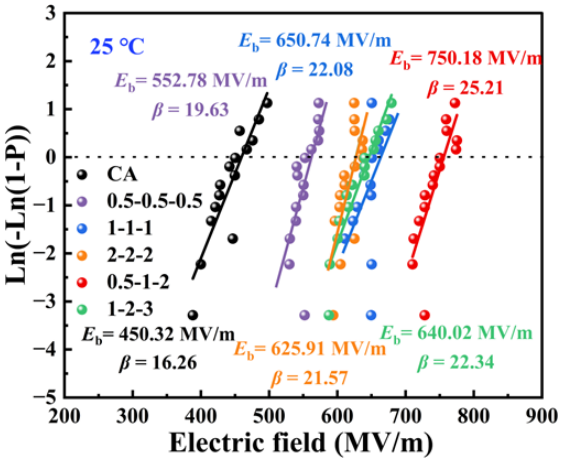

Fig. S12 Weibull distribution analysis of the E_b for different films at 25 ℃ as indicated.

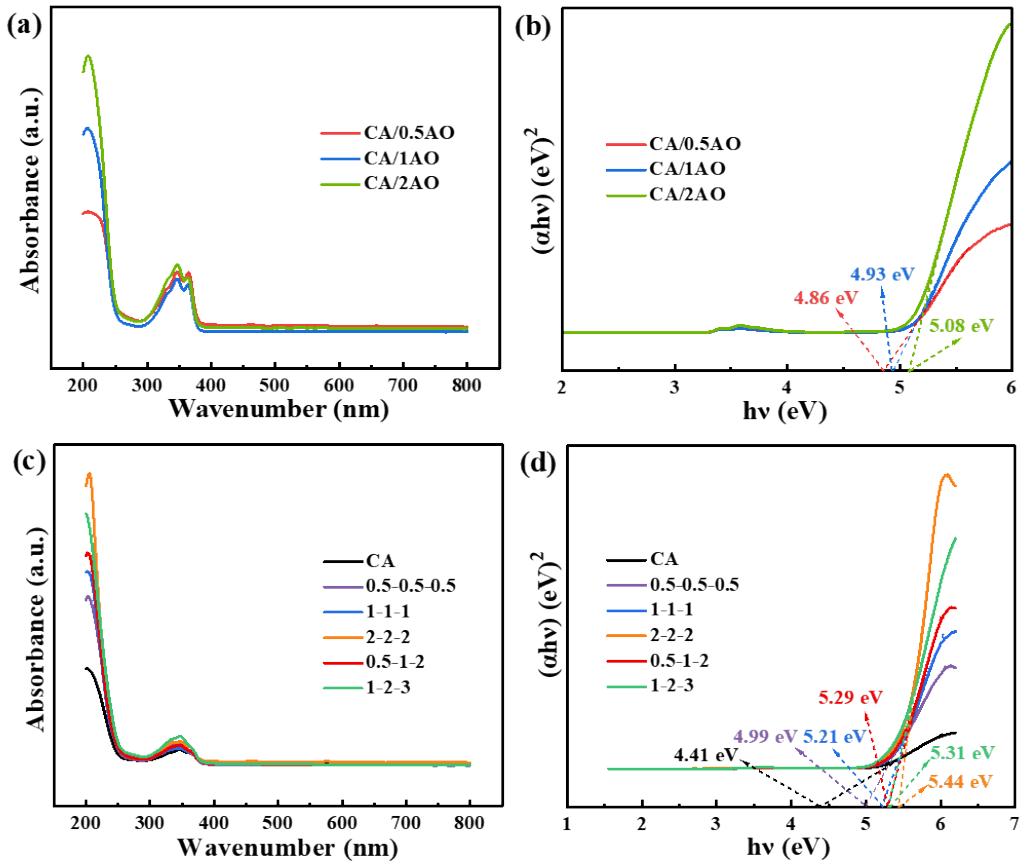

Fig. S13 (a, c) UV-visible absorption spectra of different films. (b, d) Band gap diagram of UV-visible absorption spectrum calculation of different films.

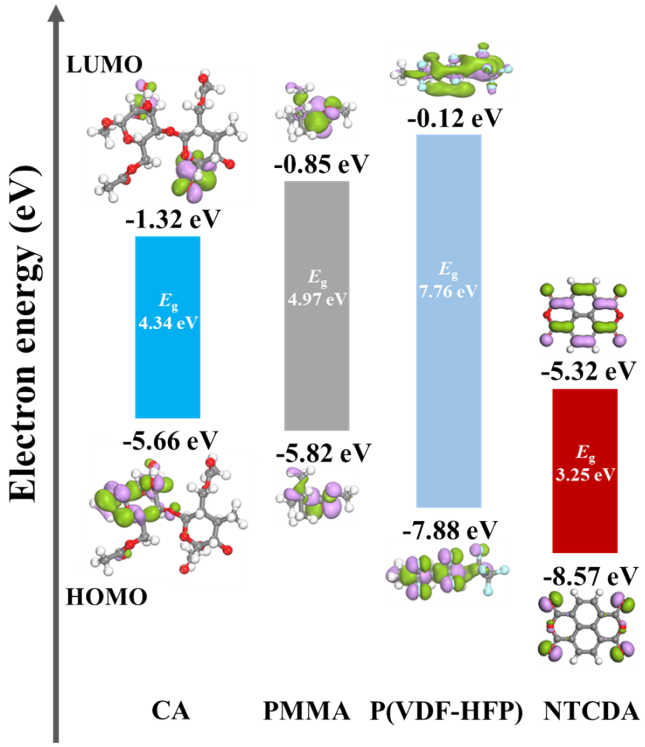

Fig. S14 The electrostatic potential distribution of CA, PMMA, P(VDF-HFP) and NTCDA.

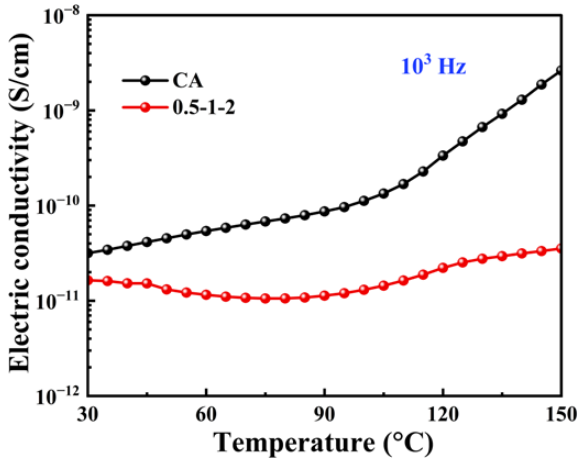

Fig. S15 The temperature dependence of conductivity at 10^3 Hz for CA and 0.5-1-2 composite film.

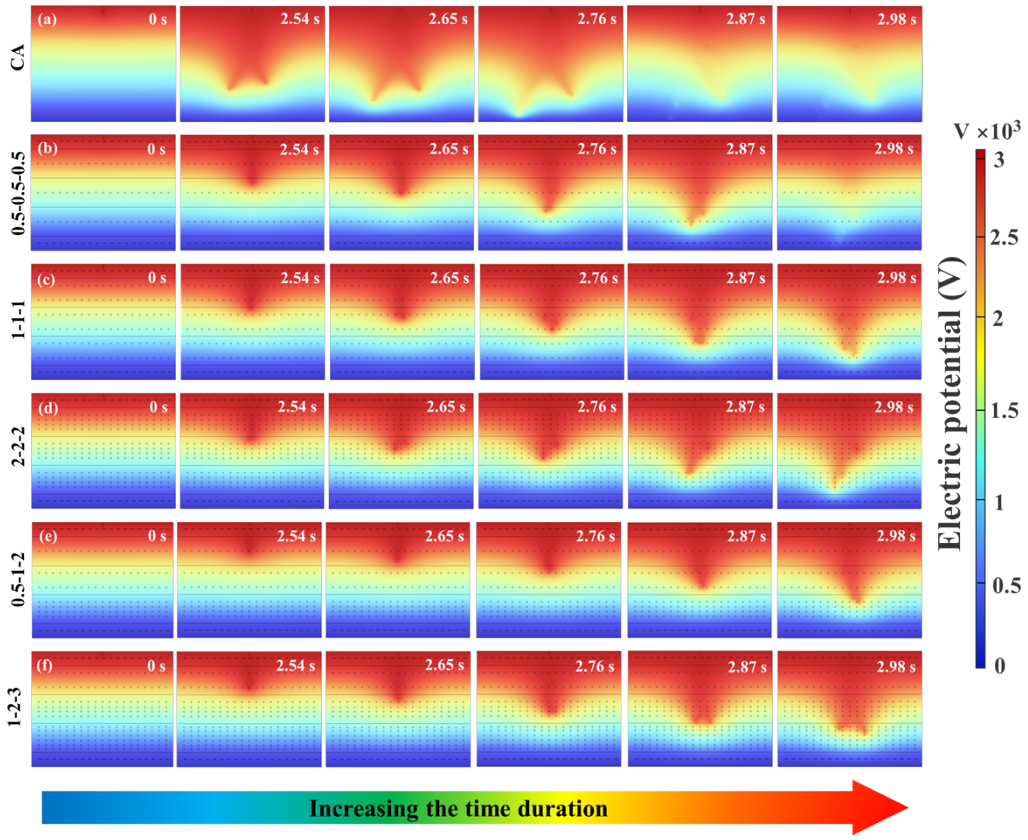

Fig. S16 The real-time evolution of the electric potential in different composite films.

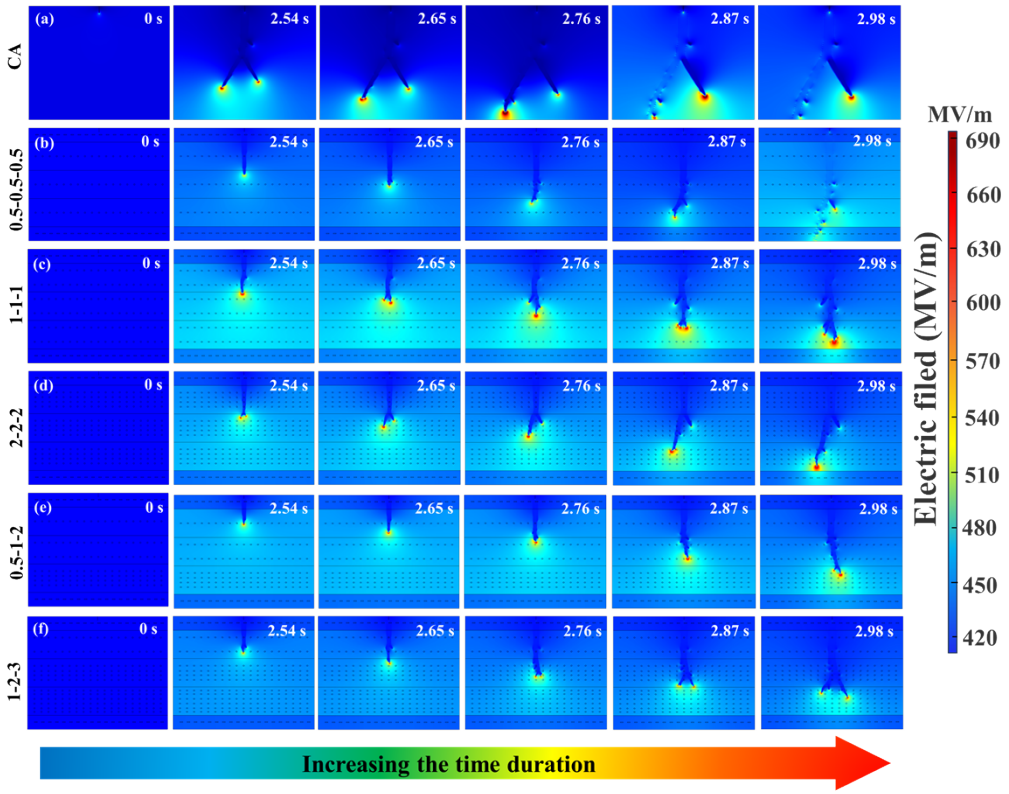

Fig. S17 The real-time evolution of the electric field distributions with electrical trees propagation in different composite films.

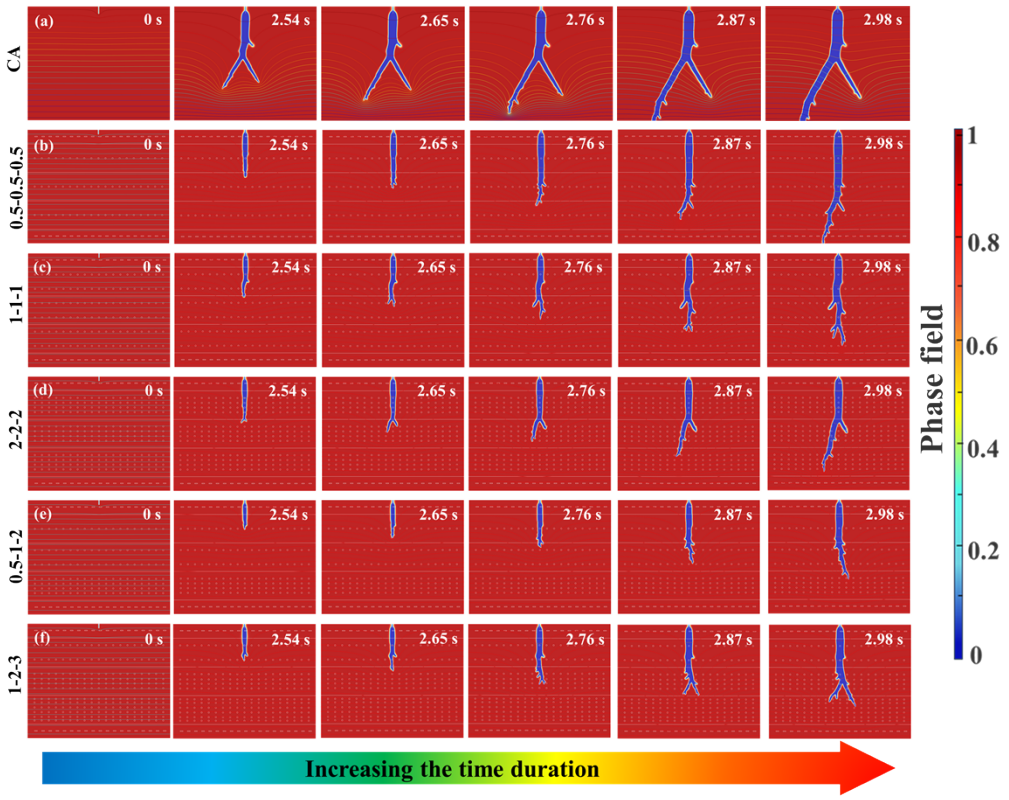

Fig. S18 The real-time evolution of the phase field distributions with electrical trees propagation in different composite films.

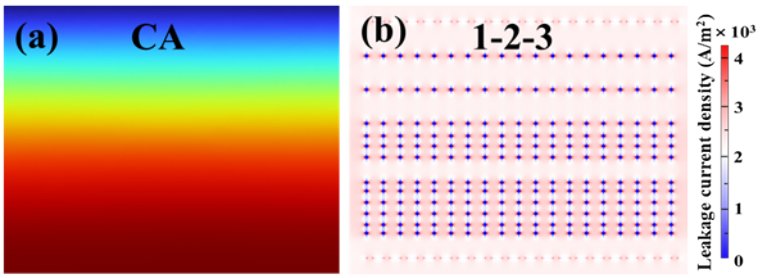

Fig. S19 Leakage current density simulated of (a) pure CA and (b) 1-2-3 composite film.

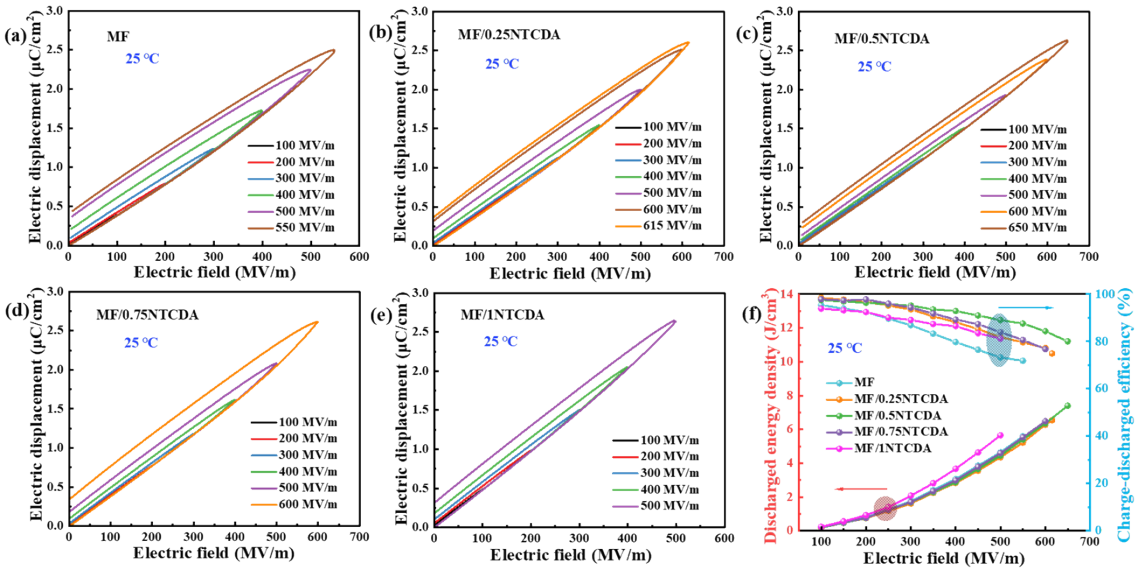

Fig. S20 (a-e) The unipolar *D-E* loops at different electric fields of MF and MF/NTCDA dielectric films at 25 ℃. (f) Comparison of energy storage properties among the different dielectric films at 25 ℃.

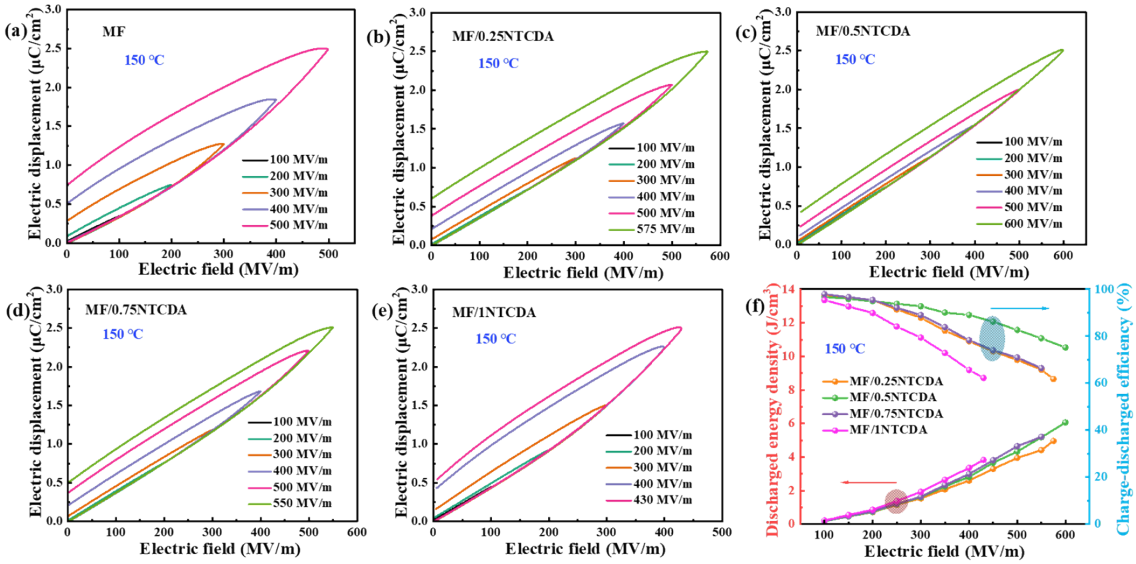

Fig. S21 (a-e) The unipolar *D-E* loops at different electric fields of MF and MF/NTCDA dielectric films at 150 ℃. (f) Comparison of energy storage properties among the different dielectric films at 150 ℃.

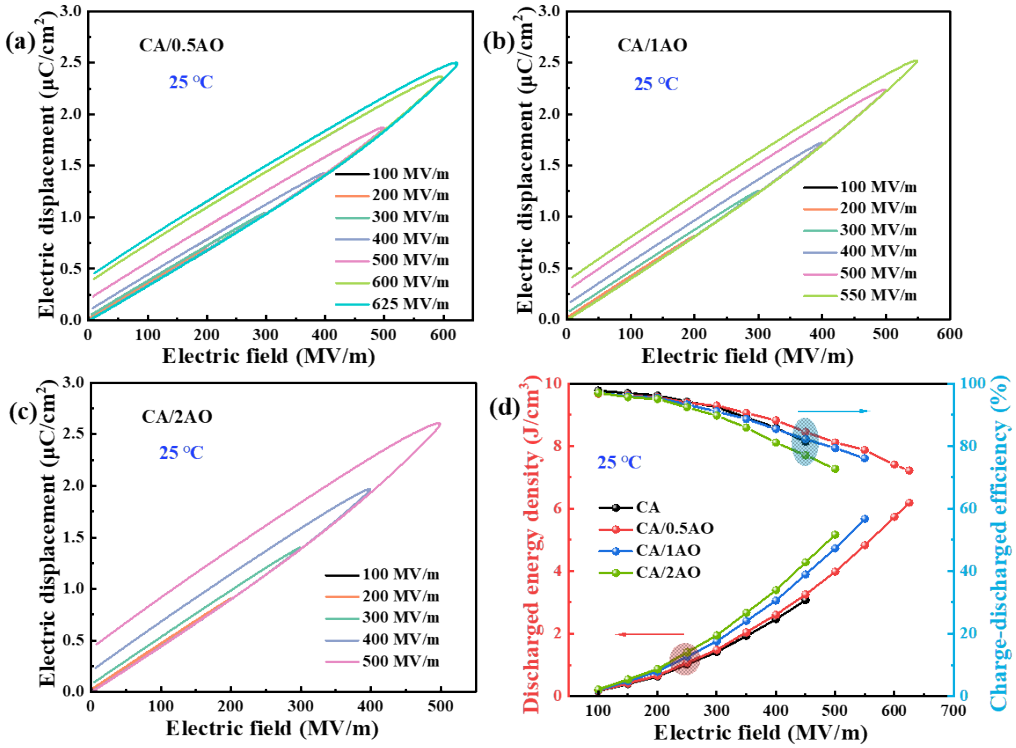

Fig. S22 (a-c) The unipolar *D-E* loops at different electric fields of CA/AO dielectric films at 25 °C. (d) Comparison of energy storage properties among the different dielectric films at 25 °C.

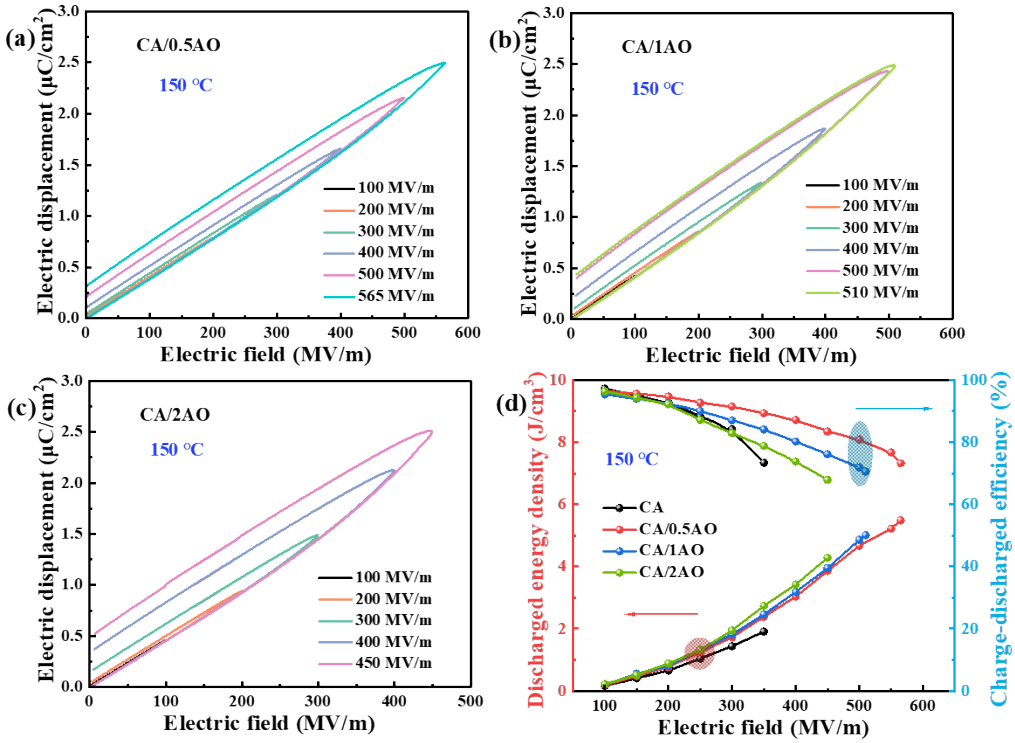

Fig. S23 (a-c) The unipolar *D-E* loops at different electric fields of CA/AO dielectric films at 150 °C. (d) Comparison of energy storage properties among the different dielectric films at 150 °C.

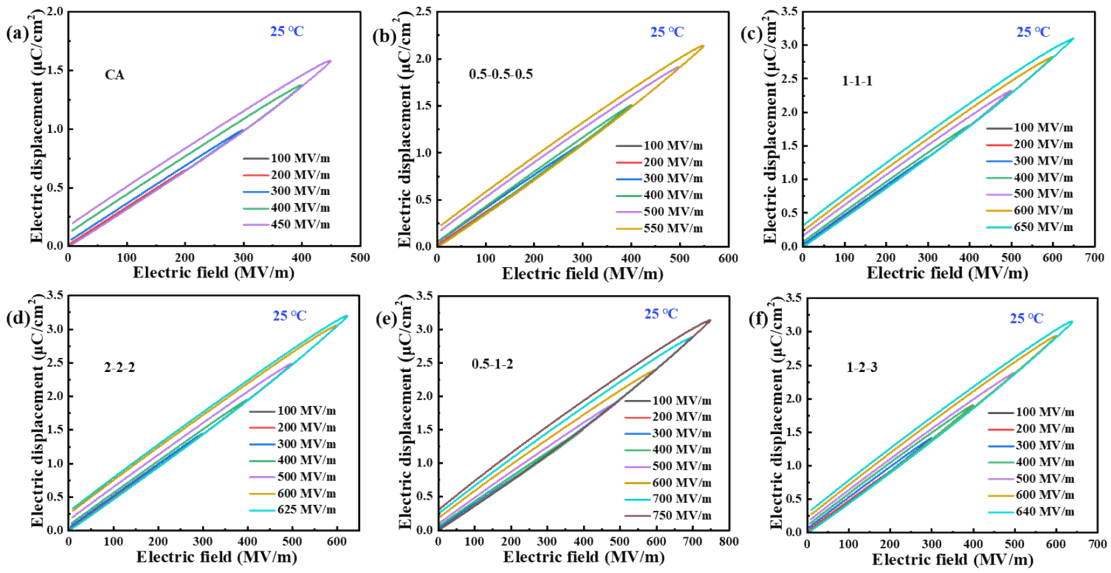

Fig. S24 The unipolar *D-E* loops at different electric fields of different dielectric films at 25 ℃ as indicated.

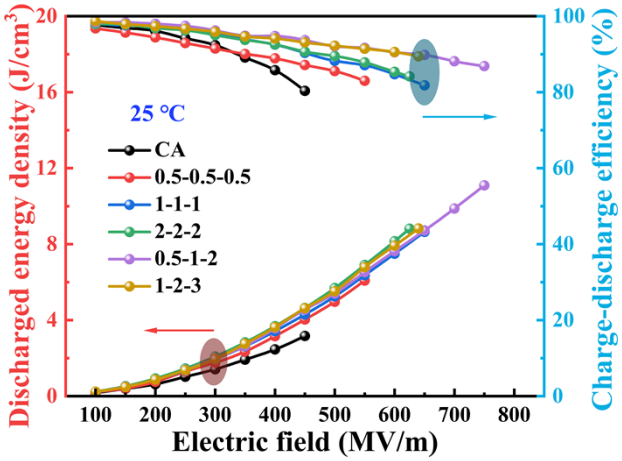

Fig. S25 Comparison of energy storage properties among the different dielectric films as indicated at 25 ℃.

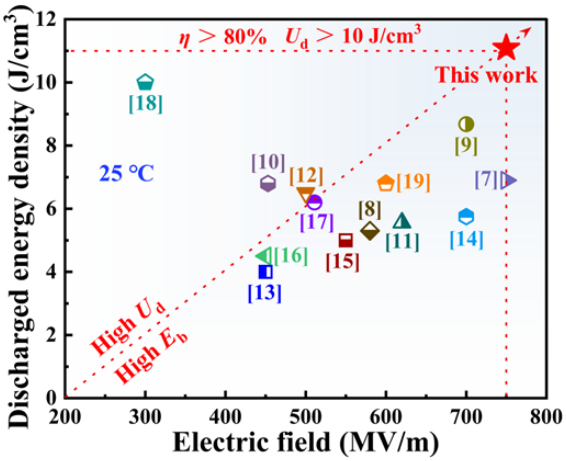

Fig. S26 Comparison of U_d at 25 ℃ between 0.5-1-2 and other films reported in literatures.[7-19]

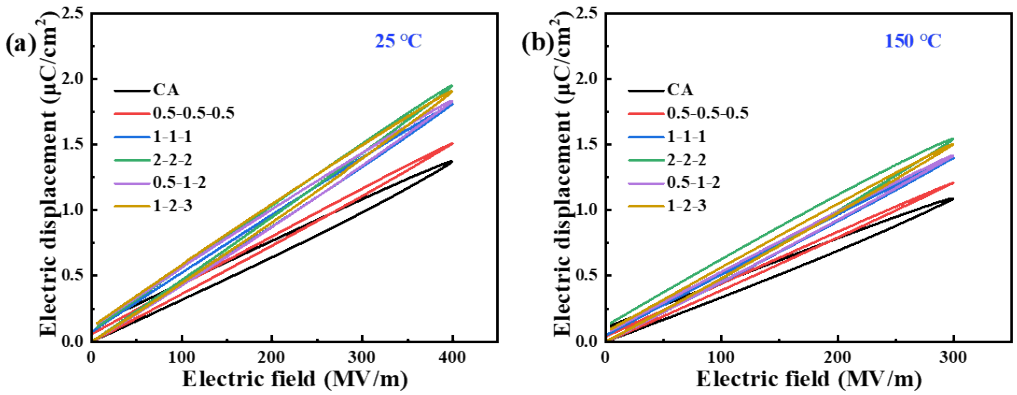

Fig. S27 The *D-E* loops of different samples at (a) 400 MV/m and 25 ℃, (b) 300 MV/m and 150 ℃.

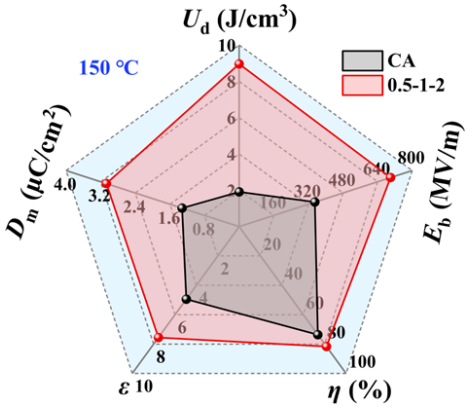

Fig. S28 Comparison of the dielectric and capacitive parameters of CA and 0.5-1-2 composite film at 150 ℃.

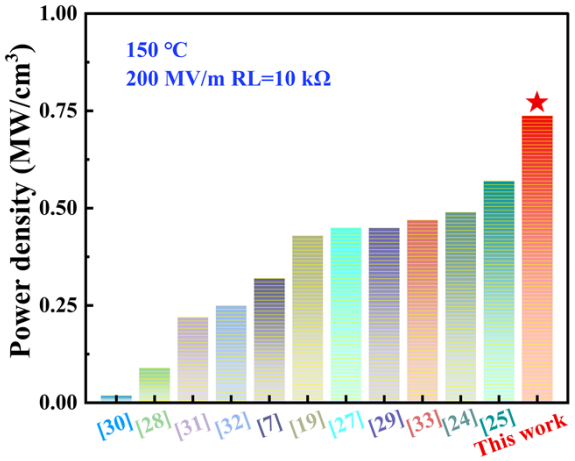

Fig. S29 Comparison of power density between 0.5-1-2 and other films reported in literatures.[7,19,24,25,27-33]

Table S1. Comparison of the dielectric and capacitive parameters among the different five-layer composite films at 150 ℃.

Samples	ε	D_m (μC cm^{-2})	E_b (MV m^{-1})	U_d (J cm^{-3})	η (%)
CA	4.94	1.32	352.67	1.91	73.56
0.5-0.5-0.5	6.53	2.95	450.72	3.66	82.64
1-1-1	7.17	3.01	600.11	6.17	77.13
2-2-2	8.48	3.09	550.24	7.05	81.44
0.5-1-2	7.55	3.07	700.71	8.96	81.65
1-2-3	8.13	2.97	563.82	6.58	79.21

Table S2. Comparison of power density between 0.5-1-2 and other films reported in literatures.[7,19,24,25,27-33]

Samples	Power density (MW cm^{-3})	References
AlO-PEI/FTO-A-AlO	0.019	[30]
PEI/AOC	0.09	[28]
F4-TCNQ/PEI	0.22	[31]
NSCPDs/PEI	0.25	[32]
PPS-200 nm Al_2O_3	0.32	[7]
c-PPTA/PEI	0.43	[19]
PTFMB-SI	0.45	[27]
TiO_2@Au@AlO_x@Au	0.45	[29]
DE/P(VDF-HFP)-PMMA-DE/P(VDF-HFP)	0.47	[33]
GLC/PEI-PEI-GLC/PEI	0.49	[24]
Al_2O_3-BT@SiO_2/PI-Al_2O_3	0.57	[25]
0.5-1-2	**0.738**	**This work**

Note: AlO: Alumina (Al_2O_3); PEI: Polyetherimide; FTO: Fe_2O_3–TiO_2; A: Aligned; AOC: Aluminum macrocycle; F4-TCNQ: 2,3,5,6-tetrafluoro-7,7,8,8-tetracyanoquinodimethane; NSCPDs: N and S atom-doped carbon polymer dots; PPS: Polyphenylene sulfide; c-PPTA: Carboxylated poly(p-phenylene terephthalamide); PTFMB: Siloxane-fluorine-containing polyamide; DE: Dielectric elastomers; P(VDF-HFP): Poly(vinylidene fluoride-co-hexafluoropropene); PMMA: Poly(methyl methacrylate); GLC: Glucose; BT: Barium titanate.

Table S3. Comparison of capacitive performances between this work and other previous reports.

Samples	E_b (MV m^{-1})	U_d (J cm^{-3})	References
2MF-CA-2MF	600	6.48	20
NTCDA/PEI−KLNS/PEI−NTCDA/PEI	570	5	8
PEI−PEI/CQDs−PEI	500	4	21
PI/PEIs/PI	390	3	14
BNNSs/PEI-$BaTiO_3$/PEI-BNNSs/PEI	450	7.36	22
PEI/PESU 9 Lays	550	5	23
PEI−CEC−PEI	400	3	10
PEI−GLC/PEI−PEI	650	6.52	24
PI−CPC	700	6.8	7
Al_2O_3−PEI−Al_2O_3	550	4	18
BN-BCB−BT-BCB−BN-BCB	500	4.64	17
Al_2O_3−BT@SiO_2/PI−Al_2O_3	400	3	25
h-BNNS/PEI−ST@AO/PEI−h-BNNS/PEI	400	4.14	26
MF/NTCDA-CA/AO-MF/NTCDA	**700.71**	**8.96**	**This work**

Notes：MF: Polymethyl methacrylate/poly (vinylidene fluoride-co-hexafluoropropylene); CA: Cellulose acetate; NTCDA: 1,4,5,8-naphthalenetetracarboxylic dianhydride; KLNS: Kaolinite nanosheets; PEI: Polyetherimide; CQDs: Carbon quantum dots; PI: Polyimide; PEIs: Polyetherimides; BNNS: Boron nitride nanosheets; $BaTiO_3$: Barium titanate; PESU: Polyethersulfone; CEC: Cyanoethyl cellulose; GLC: Glucose; CPC: Cross-property connection; Al_2O_3: Alumina; BN-BCB: Benzocyclobutene modified BN; BT-BCB: Benzocyclobutene modified barium titanate; SiO_2: Silicon oxide; h-BNNS: Hexagonal boron nitride nanosheets; ST@AO: Strontium titanate@alumina nanoparticles.

● References

1 P. Yin, L. Lei, Q. Y. Tang, D. Dastand, Y. Liu, H. Wang, and Z. C. Shi, *Energy Storage Mater.*, 2025, **77**, 104213.

2 K. Fan, X. Li, X. Y. Liu, X. He, and Z. M. Dang, *Adv. Mater.*, 2025, **37**(20), 2417181.

3 Y. D. Jiang, X. Zhang, Z. H. Shen, X. H. Li, J. J. Yan, B. W. Li, and C. W. Nan, *Adv. Funct. Mater.*, 2020, **30**(4), 1906112.

4 M. Z. Fan, P. H. Hu, Z. K. Dan, J. Y. Jiang, B. Z. Sun, and Y. Shen, *J. Mater. Chem. A*, 2020, **8**(46), 24536–24542.

5 F. R. Kong, W. Y. Zhou, F. Zhang, W. W. Li, H. M. Li, Y. W. Zhu, B. Zhou, T. Yao, and B. Li, *J. Mater. Chem. A*, 2025, **13**(12), 8852–8864.

6 H. Luo, C. F. Yan, X. Liu, H. Luo, H. J. Chen, and S. Chen, *Chem. Eng. J.*, 2024, **497**, 154405.

7 M. H. Lin, J. T. Zhuo, S. W. Huang, Q. Y. Zhang, and Q. M. Zhang, *Chem. Eng. J.*, 2024, **498**, 155586.

8 S. Y. Zhou, H. Zhao, N. Zhang, L. Yin, and J. B. Bai, *Chem. Eng. J.*, 2025, **504**, 158941.

9 J. X. Chen, F. H. Ren, N. N. Yin, and J. Mao, *Chem. Eng. J.*, 2024, **479**, 147581.

10 C. Yan, H. Luo, X. Liu, Y. Liu, H. Luo, and S. Chen, *Mater. Today Sustain.*, 2023, **21**, 100310.
11 M. Liu, F. H. Liu, H. M. Qin, C. X. Xiong, H. X. Xiang, L. P. Zhu, and M. F. Zhu, *Small*, 2025, **21**(27), 2501691.
12 F. Wang, H. Wang, X. M. Shi, C. L. Diao, C. L. Li, W. K. Li, X. Liu, H. W. Zheng, H. B. Huang, and X. G. Li, *Chem. Eng. J.*, 2024, **485**, 149972.
13 D. Ai, Y. T. Han, Z. L. Xie, X. Pang, Y. Chang, H. Li, C. L. Wu, Y. H. Cheng, and G. L. Wu, *Nano Res.*, 2024, **17**(8), 7746–7755.
14 Y. J. Niu, J. F. Dong, Y. F. He, X. W. Xu, S. Li, K. Wu, Q. Wang, and H. Wang, *Nano Energy*, 2022, **97**, 107215.
15 S. Q. Yu, Y. Liu, C. L. Ding, X. Liu, Y. Liu, D. Wu, H. Luo, and S. Chen, *J. Energy Storage*, 2023, **62**, 106868.
16 J. Chen, Y. Li, Y. F. Wang, J. F. Dong, X. W. Xu, Q. B. Yuan, Y. J. Niu, Q. Wang, and H. Wang, *Compos. Sci. Technol.*, 2020, **186**, 107912.
17 D. Y. Zhao, Q. N. Cai, X. B. Zhu, W. H. Xu, Q. W. Zhou, S. Niu, Z.H. Jiang, and Y. H. Zhang, *ACS Appl. Mater. Interfaces*, 2022, **14**(37), 42531−42540.
18 S. Cheng, Y. Zhou, Y. S. Li, C. Yuan, M. C. Yang, J. Fu, J. Hu, J. L. He, and Q. Li, *Energy Storage Mater.*, 2021, **42**, 445–453.
19 J. J. Yan, H. Wang, J. Y. Zeng, X. Zhang, C. W. Nan, and S. J. Zhang, *Small*, 2023, **19**(42), 2304310.
20 F. Zhang, W. J. Hu, J. Q. Liu, N. Zhang, J. H. Yang, and Y. Wang, *Compos. Pt. B-Eng.*, 2025, **308**, 112979.
21 Z. Y. Ran, M. C. Yang, R. Wang, J. L. Li, M. X. Li, L. Meng, Y. H. Liu, J. Hu, J. L. He, and Q. Li, *Energy Storage Mater.*, 2025, **74**, 103952.
22 Z. E. Dang, Y. Lin, Q. B. Yuan, X. Y. Li, Y. J. Zhang, Y. L. Ma, Y. Wang, Q. Y. Yang, Y. F. Wang, and H. B. Yang, *Adv. Funct. Mater.*, 2024, **34**(41), 2406148.
23 C. H. Zhang, X. Tong, T. D. Zhang, Y. Zhang, Y. Q. Zhang, X. Zhang, C. Tang, and Q. G. Chi, *Chem. Eng. J.*, 2024, **491**, 151634.
24 H. Sun, T. D. Zhang, C. Yin, H. Z. Sun, C. H. Zhang, Y. Zhang, Y. Q. Zhang, C. Tang, and Q. G. Chi, *Chem. Eng. J.*, 2024, **497**, 154546.
25 J. F. Dong, R. C. Hu, Y. J. Niu, L. Sun, L. T. Li, S. Li, D. S. Pan, X. W. Xu, R. Gong, J. Cheng, Z. Z. Pan, Q. Wang, and H. Wang, *Nano Energy*, 2022, **99**, 107314.
26 H. X. Chen, Z. B. Pan, Q. G. Chi, M. H. Yang, Y. Cheng, X. P. Ding, J. J. Liu, J. H. Yu, and Z. M. Dang, *J. Mater. Chem. A*, 2022, **10**(3), 1579–1587.
27 X. Li, K. Fan, J. Y, He, S. Y. Sun, Y. N. Chai, Z. M. Dang, and X. Y. Liu, *Energy Environ. Sci.*, 2025, **18**, 7589–7602.
28 Z. B. Pan, Y. Chen, Z. C. Li, X. Pang, P. Wang, X. Fan, H. X. Chen, J. J. Liu, J. F. Luo, J. H. Yu, M. H. Yang, J. W. Zhai, and W. P. Li, *Energy Environ. Sci.*, 2025, **18**(9), 4405–4415.
29 Z. L. Ren, L. Lei, L. W. Zhu, S. M. Xia, R. H. Fan, D. Dastan, H. Z. Cui, and Z. C. Shi, *Adv. Funct. Mater.*, 2025, **35**(11), 2417156.
30 Z. Li, J. Wang, J. J. Zou, S. X. Li, X. Zhen, Z. H. Shen, B. W. Li, X. Zhang, and C. W. Nan, *Mater. Horizons*, 2024, **11**(18), 4472–4481.
31 X. N. Li, H. Luo, Y. T. Wan, B. Peng, Y. Liu, S. Chen, and D. Zhang, *Chem. Eng. J.*, 2024, **488**, 150874.
32 H. Wang, H. Luo, R. Guo, J. J. Peng, G. H. He, D. Hu, X. W. Yang, and D. Zhang, *Small*, 2025, **21**, 2504788.
33 J. Chen, Y. F. Wang, X. W. Xu, Q. B. Yuan, Y. J. Niu, Q. Wang, and H. Wang, *J. Mater. Chem. A*, 2019, **7**(8), 3729-3736.